Ultrafast near-infrared spectroscopic study of coherent phonons in the phase-separated manganite La$_{1/4}$Pr$_{3/8}$Ca$_{3/8}$MnO$_3$

Kyeong-Jin Jang,[1] Jongseok Lim,[1] Jaewook Ahn,[1,*] Ji-Hee Kim,[2] Ki-Ju Yee,[2] and Jai Seok Ahn[3,†]

[1]*Department of Physics, Korea Advanced Institute of Science and Technology, Daejeon 305-701, Korea*
[2]*Department of Physics, Chungnam National University, Daejeon 305-764, Korea*
[3]*Department of Physics and RCDAMP, Pusan National University, Pusan 609-735, Korea*

We report the generation of coherent optical and acoustic phonons in mixed valent manganite La$_{1/4}$Pr$_{3/8}$Ca$_{3/8}$MnO$_3$ using femtosecond infrared pump-probe spectroscopy. Temperature-dependent measurements of the time-resolved optical reflectance, obtained over a range of 5–300 K, revealed that the energy of the photoexcited electrons dissipated during relaxation to acoustic phonons, in the high-temperature paramagnetic phase, and to optical phonons, in the low-temperature charge-ordering phase. Analysis of the temperature-dependent behavior reveals that the modal amplitudes of the coherent phonons appear strongly correlated with the charge-ordering phase.

PACS number(s): 78.47.−p, 75.47.Lx, 63.20.−e

I. INTRODUCTION

Ultrafast optical-pulse excitation of condensed matter produces several types of coherent phonon oscillations that can be measured as oscillatory changes in the material's optical properties. Coherent phonons originate from coherently excited lattice vibrations resulting from the superposition of optical or acoustic phonon modes. These coherent phonons have been widely used to study the material properties of semimetals, semiconductors, superconductors, quantum dots, and carbon nanotubes.[1–7] Recently, coherent phonons have been used to probe structural phase transitions,[8,9] to generate terahertz radiation,[10] and to switch x-ray pulses.[11]

The generation of coherent phonons depends on the lattice structure and the excited carrier distribution. Thus, the specific generation mechanism for a given material determines the type of coherent phonons. Several types of generation mechanisms for coherent phonons exist, including impulsive-stimulated Raman scattering,[12] Brillouin oscillations, transient screening of the surface depletion field,[1] and, the most important generating mechanism in optically opaque bulk materials, displacive excitation of coherent phonons (DECPs).[2,3,13]

In DECP, a laser pulse excites the electrons, thereby shifting the equilibrium nuclear positions and generating coherent lattice vibrations relative to the new equilibrium nuclear positions. The coherent phonon amplitude Q in the presence of a nonequilibrium electron distribution is

$$\frac{\partial^2 Q}{\partial t^2} + \omega^2 Q = f(n_e, T_e, \ldots), \qquad (1)$$

where n_e and T_e are the density and temperature of the pumped electrons, respectively. The time dependence of Q, determined from the measured optical reflectivity in pump-probe spectroscopic experiments, can be described by a damped-harmonic oscillatory function, determined by the dephasing and relaxation of the coherent phonons.[14–16] The dynamic behavior of the coherent phonons is expected to be strongly coupled with their relaxation pathways to other lattice vibration modes as well as with their spin degrees of freedom. In an experiment where spin-lattice interaction is mediated by photoexcited process, the atomic displacement probed in coherent phonon oscillation results in a longer time-dependent reflectivity change. The slow decay in reflectivity appearing after dephasing of coherent phonons is strongly coupled with magnetic ordering. Therefore, we can speculate spin degree of freedom coherently survives longer than optical phonons. This dynamic behavior of coherent phonons thus opens an interesting opportunity to explore new physics in newly developed materials.

Probing coherent phonons or directly tracing particular lattice vibrations in strongly correlated materials enables the characterization of the relaxation dynamics caused by the excited energy carriers.[17] In particular, ultrafast studies of phase-separated manganite may provide a means of achieving optical control over the ground-state competition between the metallic and insulating phases. Generation of coherent phonons has been reported in La$_{1−x}$Ca$_x$MnO$_3$ (Ref. 18) and LuMnO$_3$.[19]

Here, we describe a study of phase-separated manganite La$_{1/4}$Pr$_{3/8}$Ca$_{3/8}$MnO$_3$ (LPCMO). This material is particularly interesting due to the presence of micron-sized domains consisting of charge-ordering (CO) or ferromagnetic-metallic (FMM) phases.[20] Interplays of the two LPCMO phases gives rise to very complex phase transition sequences: (I) $T < T_C$, FMM-dominant mixed phases with long-range CO and long-range FMM character, which are electrically metallic; (II) $T_C < T < T_{CO}$, CO-dominant mixed phases with short-range CO and short-range FMM behavior, which are electrically semiconducting; and (III) $T > T_{CO}$, which is a simple paramagnetic insulating phase. Thus, the temperature-dependent time-resolved measurement of phonon amplitudes is a challenging method of probing the coupled dynamics of electrons, lattice, and the spin degrees of freedom in this mixed-phase manganese material.

In this paper, we present femtosecond pump-probe reflection measurements of LPCMO in the temperature range 5–300 K. Time-resolved measurements of the optical reflectance over a wide range of temperatures revealed that the generated coherent-optical phonons were strongly coupled to

the charge-ordering domains in the CO and FMM mixed phases. Coherent acoustic phonons were simultaneously observed in strain propagation in the high-temperature paramagnetic phase. We found that the temperature-dependent responses of these two types of phonon generation were complementary. We explain this phenomenon using a gap opening and unequal Mn-O distances in the below the T_{CO}.

II. EXPERIMENTAL PROCEDURE

The LPCMO sample was synthesized from La_2O_3, Pr_6O_{11}, $CaCO_3$, and MnO_2 by sintering in ambient air up to 1400 °C for 48 h with repeated grinding and pelletizing. T_C and T_{CO} were determined as ~80 and 220 K, respectively, from a four-probe resistivity measurement under zero-magnetic field. The sample was cut and wet-polished using an Al_2O_3 emulsion for the reflectance measurements. The sample was optically pumped, then probed by 20 fs laser pulses from a cavity-dumped Ti:Sapphire laser oscillator operated at a wavelength of 780 nm (~1.6 eV) with a repetition rate of 400 kHz. The focused laser spots were 80 and 30 μm in diameter for the pump and probe pulses, respectively. The change in reflectance at the sample surface induced by the pump pulse was later measured by a weak probe pulse as a function of time delay generated by a raster-scanning shaker. The laser pump pulse fluence was maintained at less than 100 μJ/cm^2 to minimize local heating of the sample, and the probe intensity was one-tenth that of the pump pulse. The polarization of the pump beam was maintained perpendicularly to that of the probe to minimize coherent artifacts and detection noise from scattered pump beams. The sample temperature was varied from 5 to 300 K in a microscope cryostat (JANIS ST-500) cooled with liquid He.

III. RESULTS AND DISCUSSION

The photoinduced changes in reflectivity, $\Delta R/R$, measured at various temperatures, are plotted in Fig. 1 as a function of time delay. $\Delta R/R$ decreases abruptly at zero time delay and relaxes very slowly. The measured results are plotted on two different time scales; Fig. 1(a) shows the ultrafast dynamics within 3.5 ps and Fig. 1(b) shows the rather slower process that took place over 40 ps. Oscillatory behaviors in $\Delta R/R$ were observed on two distinct time scales. The first oscillatory behavior, shown in Fig. 1(a), had a period of ~400 fs and dephased within a few picoseconds. The second oscillation, shown in Fig. 1(b), had a period of ~26 ps. The measured $\Delta R/R$ as a function of both temperature and time delay is shown in Fig. 1(c). There are two distinct features in the plot of $\Delta R/R$; (i) a crossover observed at 3 ps as a function of time delay and (ii) the oscillatory dynamics, which are localized in the midtemperature region, around 130 K.

The data were empirically fitted using the equation

$$\frac{\Delta R}{R} = C + \sum_{i=1,2} A_i e^{-\beta_i t} + \sum_{i=1,2} B_i e^{-\gamma_i t} \cos(\omega_i t + \phi_i), \quad (2)$$

which describes the oscillatory decay. Here ω_i and γ_i are the angular frequencies and damping constants of the coherent
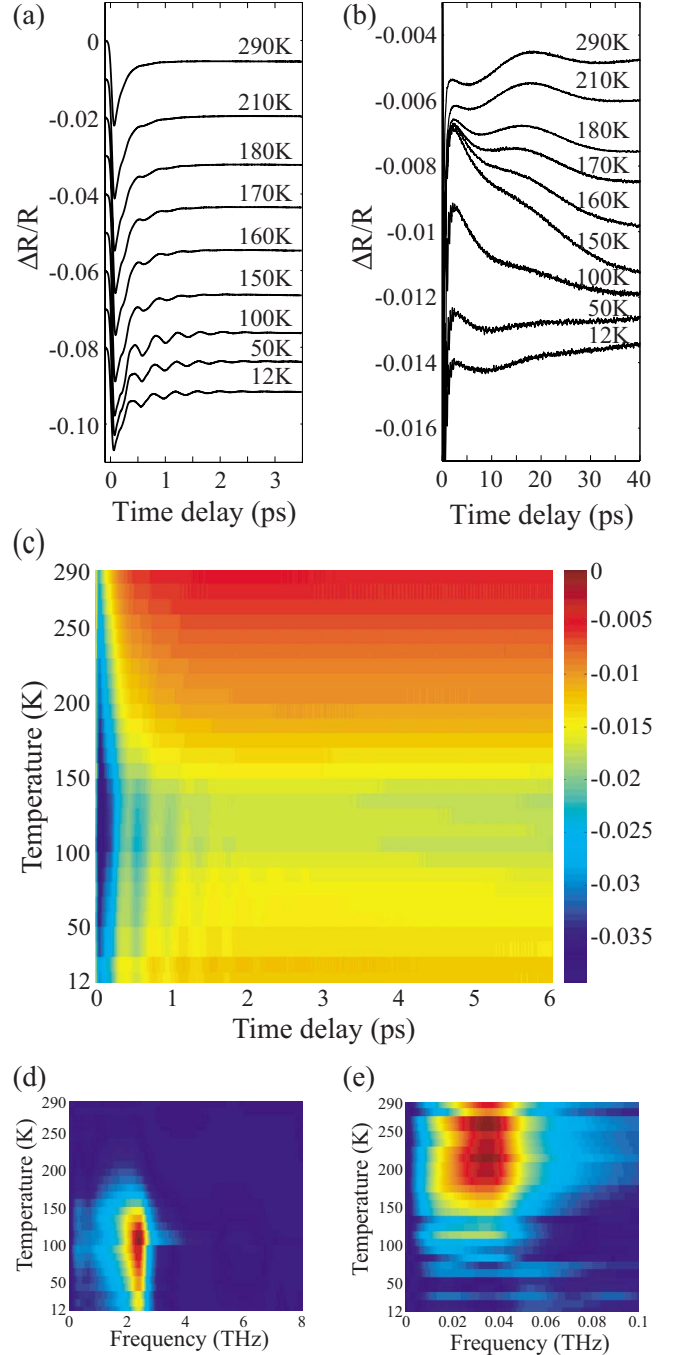
FIG. 1. (Color online) Photoinduced change in reflectivity $\Delta R(t)/R$ of $La_{1/4}Pr_{3/8}Ca_{3/8}MnO_3$ plotted as a function of time delay for various temperatures. (a) Fast oscillatory decay at a frequency of 2.5 THz (coherent optical phonon). (b) Slow oscillatory decay at a frequency of 34.7 GHz (strain pulse propagation of the acoustic phonon). (c) The measured $\Delta R(t)/R$ in the first 6 ps time window is plotted as a two-dimensional function of time delay and temperature. The reflectivity data in (a) and (b) are shifted along the vertical axis for clarity. (d) and (e) are Fourier-transformed spectra of fast and slow oscillatory decays in (a) and (b), respectively.

oscillations and β_i are the decay rates. To obtain the ω_is, the time series data were Fourier transformed, yielding two characteristic frequencies, 2.5 THz (fast mode) and 34.7 GHz (slow mode). The temperature dependent changes of the am-
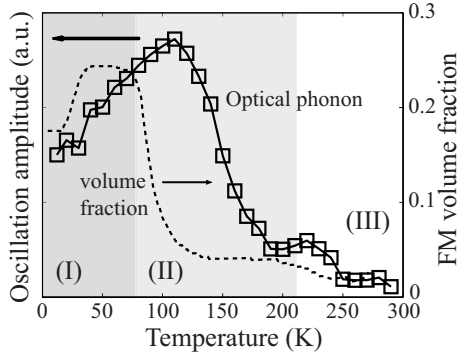
FIG. 2. Temperature dependence of the amplitude of the 2.5 THz oscillation ($B_1(T)$). As the temperature decreased, the amplitude increased near T_{CO} and subsequently decreased below 120 K. The dashed curve indicates the change in volume fraction of the LPCMO metallic phase, suggesting a correlation between the 2.5 THz coherent mode and the charge ordering phase (see text).

plitudes of the modes are plotted in Figs. 2 and 3.

A. Coherent optical phonon

The fast oscillatory behavior of $\Delta R/R$ formulated in Eq. (2) is consistent with a reflectance change characteristic of a DECP mechanism,[3] which is a good candidate for the generation of coherent optical phonons in LPCMO. The DECP mechanism describes oscillatory changes in reflectance as resulting from a change in the electronic energy distribution due to NIR absorption at the excitation wavelength. After a short pulse excitation, electrons reach quasiequilibrium much faster than nuclei, so the $k \sim 0$ modes are coherently excited. The oscillation in $\Delta R(t)$ originates from a change in the quasiequilibrium nuclear coordinates $Q_0(t)$. The equation of motion for the coordinates $Q(t)$ is

$$\frac{\partial^2 Q}{\partial t^2} = -\omega_1^2[Q(t) - Q_0(t)] - 2\gamma_1 \frac{\partial Q}{\partial t}, \quad (3)$$

where ω_1 and γ_1 are the angular frequency and the damping constant of the mode, respectively. If, in Eq. (3), $\gamma_1 \ll \omega_1$ and the width of the pulse are assumed to be sufficiently small, $\Delta R/R$ becomes[3]

$$\frac{\Delta R}{R} = A_0 e^{-\beta_1 t} + B_0 \frac{\omega_1^2}{\omega_1^2 + \beta_1^2 - 2\beta_1\gamma_1}$$
$$\times \left[e^{-\beta_1 t} - e^{-\gamma_1 t} \left\{ \cos(\Omega t) - \frac{\beta_1'}{\Omega} \sin(\Omega t) \right\} \right], \quad (4)$$

where $\Omega \equiv \sqrt{\omega_1^2 - \gamma_1^2}$ and $\beta_1' = \beta_1 - \gamma_1$. If β_1 is sufficiently small compared to ω_1, i.e., $\beta_1 \ll \omega_1$, $\Delta R/R$ can be described with a simple exponential decay, overlaid by a cosinelike damped oscillation, as given in Eq. (2) with the replacements: $A_1 = A_0 + B_0\omega^2/(\omega_1^2 + \beta_1^2 - 2\beta_1\gamma_1)$, $\omega_1 = \sqrt{\Omega^2 - \gamma_1^2}$, and $\phi_1 = \tan^{-1}((\beta_1 - \gamma_1)/\omega_1)$.

The DECP mechanism also predicts that only A_1 modes are generated through the relaxation of ultrafast electronic excitations.[2] A previous Raman study of LPCMO by Amelitchev *et al.* reported that the A_{1g} mode was located at
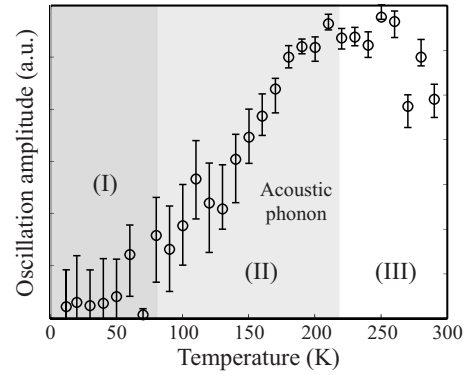
72–90 cm^{-1} ($=2.2$–2.7 THz).[21] Thus, the first dominant fast mode found in Fig. 1(a) can be assigned as a coherent A_{1g} phonon mode (i.e., a coherent Raman-active optical phonon mode). A more careful fitting of the fast oscillations reveals that there are actually two frequency components: 2.5 and 5.1 THz, and the amplitude of the 5.1 THz component is about 10% of the amplitude of the 2.5 THz component. The 5.1 THz mode is new, and, from a previous low-temperature Raman study of charge ordering in BCMO, is believed to be a Mn vibration.[22]

B. Coherent acoustic phonon

The slow oscillatory change in LPCMO reflectance, shown in Fig. 1(b), arises from the coherent superposition of acoustic modes. The propagation of a strain pulse generated by an instantaneous thermal stress was first proposed by Thomsen *et al.*[15] for films and inner reflection surfaces and also by Liu *et al.*[23] for bulk materials. In Liu's model, a strained layer generated at the surface propagates with the acoustic phonon wave speed $v_s n$, such that the interference produced by the reflected probe pulse at the surface and at $z = v_s\tau_d$ (after time delay τ_d) shows an oscillatory behavior. Then, Maxwell's equations for the probe electric field $\tilde{E}(z,t)$ in the slowly varying envelope approximation are given as

$$\frac{\partial^2 \tilde{E}(z,t)}{\partial z^2} + \frac{\omega_{pr}^2}{c^2}[n_0 + \delta n(z,t)]^2 \tilde{E}(z,t) = 0, \quad (5)$$

where ω_{pr} is the center frequency of the probe pulse, n_0 is the index of refraction, and δn is the index change due to strain. Then, the differential reflectance $\Delta R/R$ for the longitudinal-acoustic phonon is given by

$$\frac{\Delta R}{R}(\omega_{pr},t) \propto \frac{\omega_{pr}}{c} \cos\left(\frac{2n_0\omega_{pr}}{c} v_s t + \phi \right), \quad (6)$$

where $\phi (=\phi_2)$ is the phase angle. The oscillation period of the differential reflectivity depends on the probe wavelength λ_{probe}, i.e., $T = \lambda_{probe}/(2n_0 v_s)$, where v_s is the sound velocity. Equation (6) shows the same temporal behavior as the slow oscillatory component of Eq. (2). From fits to the measured data, T and ϕ_2 are extracted. The phase ϕ_2 was measured to be zero. The oscillation period T appears weakly temperature

FIG. 3. Temperature dependence of the modal amplitude of the 34.7 GHz oscillation ($B_2(T)$).
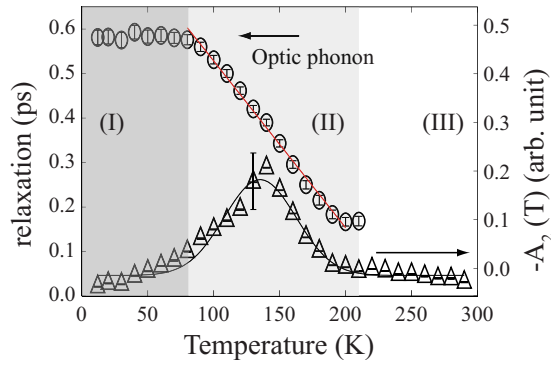
FIG. 4. (Color online) Relaxation time $(1/\gamma_1)$ of the fast oscillations (circles), and the slow decay term (A_2) (triangles), obtained using the empirical formula (2).

dependent, which is consistent with the temperature dependence of the Fourier transformed spectra of slow oscillatory decay in Fig. 1(e). Coherent acoustic phonons in charge-ordering phase have been observed with similar oscillation frequencies in experiments with similar compounds $La_{0.42}Ca_{0.58}MnO_3$ and $La_{0.50}Ca_{0.50}MnO_3$.[18] The weak temperature dependence in LPCMO is inconsistent with the case of $LuMnO_3$,[19] where a strong temperature dependence of T was reported and was interpreted with rapid change in the index n_0.

C. Charge-ordering phase and relaxation time

Figure 4 shows the relaxation time of the fast oscillations, as well as the slow nonoscillatory decay amplitude. The slow nonoscillatory decay A_2 shows peak behavior at ~ 130 K; interestingly, this is the temperature where the system consists of many small blocks of short-range FMM and CO phases and a very high configuration entropy. This suggests that the system relaxes through much slower or nonoscillatory channels, such as lattice-spin coupled relaxation. Figures 2 and 3 also show an interesting behavior of the oscillation amplitudes in the CO phase; as the temperature increases, the amplitude of the fast oscillation decreases, while that of the slow oscillation increases. At temperatures below T_{CO}, the phonon amplitude decreases as the charge ordering is formed. On the other hand, the amplitude of the

fast-oscillating optical-phonon modes show the opposite behavior near T_{CO}. The optical mode amplitude gradually increases when the temperature is in range (II) and the charge-ordering domains become long ranged.

The coherent-optic phonon mode requires a CO phase, which has unequal Mn-O distances. The metallic phase, with its equal Mn-O distances, does not have modes for coherent-optic phonon generation. Thus, the coherent-optic mode amplitude is expected to depend on the CO state volume fraction and also on the size of the Mn-O bond distortion (or Jahn-Teller distortion). For larger Mn-O distortion, the generation of a larger amplitude coherent-optic phonon mode is expected. Therefore, as metallic behavior becomes important near T_C, coherent-optical phonon generation is hindered. This behavior is clearly seen from the optical-phonon relaxation time $(1/\gamma_1)$ in Fig. 4; it increases monotonically from T_{CO} to T_C but reaches a saturated status below T_C. We note that the optical phonon amplitude reaches its peak at the temperature where the rapid change in FMM domain volume fraction occurs[24] and the pump pulse generates carriers and metallic-volume fraction increases. As a result, the equilibrium position of the A_{1g} mode is modified again, and coherent optic phonons are generated weakly.

IV. CONCLUSIONS

We examined the ultrafast dynamics of photoinduced coherent phonons in phase-separated LPCMO. We observed coherent phonons with frequencies of 2.5 THz, 5.1 THz, and 34.7 GHz. The slowest coherent oscillation, corresponding to an acoustic phonon, was found in the high temperature phase, above T_{CO}, whereas the faster modes, corresponding to optical phonons, were found in the low-temperature charge-ordering phase, below T_{CO}. Analysis of DECP and strain-pulse propagation reveals that the modal amplitudes of the coherent phonons appear strongly correlated with the charge-ordering phase.

*jwahn@kaist.ac.kr

†jaisahn@pnu.ac.kr

[1] G. C. Cho, W. Kütt, and H. Kurz, Phys. Rev. Lett. **65**, 764 (1990).

[2] T. K. Cheng, S. Vidal, M. J. Zeiger, G. Dresselhaus, M. S. Dresselhaus, and E. P. Ippen, Appl. Phys. Lett. **59**, 1923 (1991).

[3] H. J. Zeiger, J. Vidal, T. K. Cheng, E. P. Ippen, G. Dresselhaus, and M. S. Dresselhaus, Phys. Rev. B **45**, 768 (1992).

[4] J. Demsar, B. Podobnik, V. V. Kabanov, T. Wolf, and D. Mihailovic, Phys. Rev. Lett. **82**, 4918 (1999).

[5] T. Kise, T. Ogasawara, M. Ashida, Y. Tomioka, Y. Tokura, and

M. Kuwata-Gonokami, Phys. Rev. Lett. **85**, 1986 (2000).

[6] R. D. Averitt, A. I. Lobad, C. Kwon, S. A. Trugman, V. K. Thörsmolle, and A. J. Taylor, Phys. Rev. Lett. **87**, 017401 (2001).

[7] A. I. Lobad, R. D. Averitt, C. Kwon, and A. J. Taylor, Appl. Phys. Lett. **77**, 4025 (2000).

[8] T. Kohmoto, K. Tada, T. Moriyasu, and Y. Fukuda, Phys. Rev. B **74**, 064303 (2006).

[9] H. T. Kim, Y. W. Lee, B. J. Kim, B. G. Chae, S. J. Yun, K. Y. Kang, K. J. Han, K. J. Yee, and Y. S. Lim, Phys. Rev. Lett. **97**, 266401 (2006).

[10] Y. C. Shen, P. C. Upadhya, E. H. Linfield, H. E. Beere, and A. G. Davies, Phys. Rev. B **69**, 235325 (2004).

[11] M. F. DeCamp, D. A. Reis, P. H. Bucksbaum, B. Adams, J. M. Caraher, R. Clarke, C. W. S. Conover, E. M. Dufresne, R. Merlin, V. Stoica, and J. K. Wahlstrand, Nature (London) **413**, 825 (2001).

[12] Y.-X. Yan and K. A. Nelson, J. Chem. Phys. **87**, 6257 (1987).

[13] R. Merlin, Solid State Commun. **102**, 207 (1997).

[14] C. Thomsen, J. Strait, Z. Vardeny, H. J. Maris, J. Tauc, and J. J. Hauser, Phys. Rev. Lett. **53**, 989 (1984).

[15] C. Thomsen, H. T. Grahn, H. J. Maris, and J. Tauc, Phys. Rev. B **34**, 4129 (1986).

[16] A. V. Kuznetsov and C. J. Stanton, Phys. Rev. Lett. **73**, 3243 (1994).

[17] M. Hase, K. Ishioka, J. Demsar, K. Ushida, and M. Kitajima, Phys. Rev. B **71**, 184301 (2005).

[18] D. Lim, V. K. Thorsmolle, R. D. Averitt, Q. X. Jia, K. H. Ahn, M. J. Graf, S. A. Trugman, and A. J. Taylor, Phys. Rev. B **71**, 134403 (2005).

[19] D. Lim, R. D. Averitt, J. Demsar, A. J. Taylor, N. Hur, and S.-W. Cheong, Appl. Phys. Lett. **83**, 4800 (2003).

[20] M. Uehara, S. Mori, C. H. Chen, and S.-W. Cheong, Nature (London) **399**, 560 (1999).

[21] V. A. Amelitchev, B. Güttler, O. Yu. Gorbenko, A. R. Kaul, A. A. Bosak, and A. Y. Ganin, Phys. Rev. B **63**, 104430 (2001).

[22] S. Yoon, M. Rübhausen, S. L. Cooper, K. H. Kim, and S.-W. Cheong, Phys. Rev. Lett. **85**, 3297 (2000).

[23] R. Liu, G. D. Sanders, C. J. Stanton, C. S. Kim, J. S. Yahng, Y. D. Jho, K. J. Yee, E. Oh, and D. S. Kim, Phys. Rev. B **72**, 195335 (2005).

[24] K. H. Kim, M. Uehara, C. Hess, P. A. Sharma, and S.-W. Cheong, Phys. Rev. Lett. **84**, 2961 (2000).